



OPEN ACCESS

EDITED BY
Thorsten Seidel,
Bielefeld University, Germany

REVIEWED BY
Wim Dejonghe,
Ascrib, United States
Anja Thoe Fuglsang,
University of Copenhagen, Denmark

*CORRESPONDENCE
Yongqing Yang
yangyongqing@cau.edu.cn
Xiaoguang Lei
xglei@pku.edu.cn

†These authors have contributed
equally to this work

SPECIALTY SECTION
This article was submitted to
Plant Proteomics and Protein
Structural Biology,
a section of the journal
Frontiers in Plant Science

RECEIVED 20 June 2022
ACCEPTED 01 September 2022
PUBLISHED 12 October 2022

CITATION
Yang Y, Liu X, Wang X, Lv W,
Liu X, Ma L, Fu H, Song S and
Lei X (2022) Screening of protonstatin-
1 (PS-1) analogs for improved
inhibitors of plant plasma membrane
H⁺-ATPase activity.
Front. Plant Sci. 13:973471.
doi: 10.3389/fpls.2022.973471

COPYRIGHT
© 2022 Yang, Liu, Wang, Lv, Liu, Ma, Fu,
Song and Lei. This is an open-access
article distributed under the terms of
the [Creative Commons Attribution
License \(CC BY\)](https://creativecommons.org/licenses/by/4.0/). The use, distribution
or reproduction in other forums is
permitted, provided the original
author(s) and the copyright owner(s)
are credited and that the original
publication in this journal is cited, in
accordance with accepted academic
practice. No use, distribution or
reproduction is permitted which does
not comply with these terms.

Screening of protonstatin-1 (PS-1) analogs for improved inhibitors of plant plasma membrane H⁺-ATPase activity

Yongqing Yang^{1*†}, Xiaohui Liu^{2†}, Xin Wang^{2†}, Wanjia Lv^{1†},
Xiao Liu^{1†}, Liang Ma¹, Haiqi Fu¹, Shu Song¹
and Xiaoguang Lei^{2*}

¹College of Biological Sciences, China Agricultural University, Beijing, China, ²Beijing National Laboratory for Molecular Sciences, Key Laboratory of Bioorganic Chemistry and Molecular Engineering of Ministry of Education, Department of Chemical Biology, College of Chemistry and Molecular Engineering, Synthetic and Functional Biomolecules Center, and Peking-Tsinghua Center for Life Sciences, Peking University, Beijing, China

We previously identified protonstatin-1 (PS-1) as a selective inhibitor of plasma membrane H⁺-ATPase (PM H⁺-ATPase) activity and used it as a tool to validate the chemiosmotic model for polar auxin transport. Here, to obtain compounds with higher affinity than PS-1 for PM H⁺-ATPase, we synthesized 34 PS-1 analogs and examined their ability to inhibit PM H⁺-ATPase activity. The 34 analogs showed varying inhibitory effects on the activity of this enzyme. The strongest effect was observed for the small molecule PS-2, which was approximately five times stronger than PS-1. Compared to PS-1, PS-2 was also a stronger inhibitor of auxin uptake as well as acropetal and basipetal polar auxin transport in *Arabidopsis thaliana* seedlings. Because PS-2 is a more potent inhibitor of PM H⁺-ATPase than PS-1, we believe that this compound could be used as a tool to study the functions of this key plant enzyme.

KEYWORDS

arabidopsis, plasma membrane H⁺-ATPase, inhibitor, auxin transport, PS-2

Introduction

Plasma membrane (PM) H⁺-ATPases are major proton transporters in plants and fungi (Palmgren, 2001; Yang and Guo, 2018a; Yang et al., 2022); they transport protons from the cytoplasm across the plasma membrane to the apoplast using energy generated by the hydrolysis of adenosine triphosphate (ATP). This creates a proton and chemical potential gradient across the plasma membrane (Falhof et al., 2016; Yang and Guo, 2018b; Chen et al., 2021), providing a driving force for the transport of other substances including ions, organic compounds, and so on across the plasma membrane (Falhof et al.,

2016; Han et al., 2017; Yang and Guo, 2018b; Yang et al., 2021) while maintaining pH homeostasis in the cytoplasm and apoplast (Palmgren, 2001; Yang and Guo, 2018a; Havshøi and Fuglsang, 2022). The transport activity of numerous plasma membrane carrier proteins and channel proteins depends on the proton gradient and the potential gradient established by PM H⁺-ATPase (Yang et al., 2010; Yang et al., 2019a; Yang et al., 2019b; Havshøi and Fuglsang, 2022). PM H⁺-ATPase plays crucial roles in plant growth, development, and stress responses and is therefore referred to as the “master enzyme” in plants (Palmgren, 2001; Havshøi and Fuglsang, 2022).

Plants regulate many cellular processes by altering the activity of PM H⁺-ATPase. Therefore, understanding the mechanisms that regulate this pump is important for elucidating the physiological activities of plants. PM H⁺-ATPases in plants are encoded by a multigene family. For example, there are 11 homologous PM H⁺-ATPase genes (AHAs) in *Arabidopsis thaliana*, 10 in rice, 9 in tobacco, and 7 in tomato (Houlné and Boutry, 1994; Mito et al., 1996; Oufattole et al., 2000; Sperandio et al., 2011; Havshøi and Fuglsang, 2022). Because of functional redundancy, it is difficult to decipher the functions of the individual members of the PM H⁺-ATPase family. For example, in *Arabidopsis*, single PM H⁺-ATPase mutants often have no distinct phenotype, and *aha1 aha2* double mutants are embryonic lethal (Baxter et al., 2003; Gaxiola et al., 2007).

As an alternative to genetic approaches, the use of specific PM H⁺-ATPase inhibitors is an effective way to analyze the biological functions of PM H⁺-ATPases in plants. We previously identified protonstatin-1 (PS-1, (Z)-5-(furan-2-ylmethylene)-2-thioxothiazolidin-4-one), a selective inhibitor of PM H⁺-ATPase activity, from a small molecule library. PS-1 binds to the central loop of PM H⁺-ATPase and inhibits its activity (Yang et al., 2022).

The plant hormone auxin (indole-3-acetic acid [IAA]) exhibits polar transport from cell to cell (Muday and DeLong, 2001; Yang et al., 2006; Anfang and Shani, 2021; Yu et al., 2022). In the 1970s, the chemiosmotic model was proposed to explain the polar transport of auxin. According to this model, PM H⁺-ATPase plays a key role in regulating auxin transport (Rubery and Sheldrake, 1974; Went, 1974; Raven, 1975), which is mediated by diffusion and carriers, as supported by genetic analysis. To date, many auxin influx and auxin efflux transporters have been identified in plants (Zažimalová et al., 2010; Xi et al., 2019; Casanova-Sáez et al., 2021). For example, the model plant *Arabidopsis* contains four auxin influx transporters, AUX1, LAX1, LAX2, and LAX3, with AUX1 playing a major role in this process (Parry et al., 2001; Perrot-Rechenmann and Bennett, 2001; Kramer and Bennett, 2006). IAA is transported into cells through these transporters (Yang et al., 2006; Kerr and Bennett, 2007). Central to the chemiosmotic model is the dependence of IAA entry on the H⁺ gradient (or PM H⁺-ATPase), which is required for the

diffusion and active transport of IAA. The transmembrane protein kinase TMK phosphorylates the PM H⁺-ATPase which is required for H⁺-ATPase activation and auxin-induced cell wall acidification (Li et al., 2021; Lin et al., 2021). Treatment of seedlings with PS-1 blocks auxin transport and inhibits auxin-controlled growth (Yang et al., 2022). Therefore, PS-1 was successfully used to validate the chemiosmotic model,

The affinity of PS-1 for the PM H⁺-ATPase proton pump is not very high, and the half-maximal inhibitory concentration is 3.9 μM. Therefore, in the current study, we sought out compounds with increased affinity for PM H⁺-ATPase by synthesizing 34 PS-1 analogs with modified functional groups and testing their effects on PM H⁺-ATPase activity. The PS-1 analogs showed varying inhibitory effects. PS-2 had the strongest inhibitory effect on PM H⁺-ATPase activity and was approximately 5-fold stronger than PS-1. PS-2 also inhibited polar auxin transport in *Arabidopsis* seedlings more strongly than PS-1. These findings suggest that PS-2 represents a more effective tool than PS-1 for studying the functions of PM H⁺-ATPases in plants.

Results

Design and synthesis of PS-1 analogs

In order to explore the structure-activity relationships of the PS1 analogs, we divided PS-1 into two parts, the furan ring and the rhodanine ring, which are connected by an exocyclic double bond. Modification of PS-1 began with the replacement of the rhodanine ring with various five-membered heterocycle rings (1-5) (Figure 1A). We also introduced a series of chemical groups, including a propargyl group, a methyl group, or a vinyl thioethyl group, into the rhodanine ring at either the S (6-8) or N atom (9-11) (Figure 1A). In addition, we generated PS-1 derivatives with different substitutions on the furan ring (12-19) (Figure 1B) or PS-1 derivatives in which we replaced the furan ring with various aromatic or non-aromatic rings (20-31) (Figure 1B). We also reduced the double bond of PS-1 to a single bond (32) (Figure 1C) or introduced a methyl group to add steric hindrance (33) (Figure 1C). Finally, we generated a more constrained compound that was more rigid than PS-1 (34) (Figure 1C). In all, we generated 34 analogs to explore the structure-activity relationship and to identify more potent PM H⁺-ATPase inhibitors.

Verification of the inhibition of PM H⁺-ATPase activity by PS-1 analogs in isolated *Arabidopsis* vesicles

To verify the inhibitory effects of the PS-1 analogs on PM H⁺-ATPase activity, we isolated plasma membrane vesicles from *Arabidopsis* seedlings and measured the hydrolysis activity of

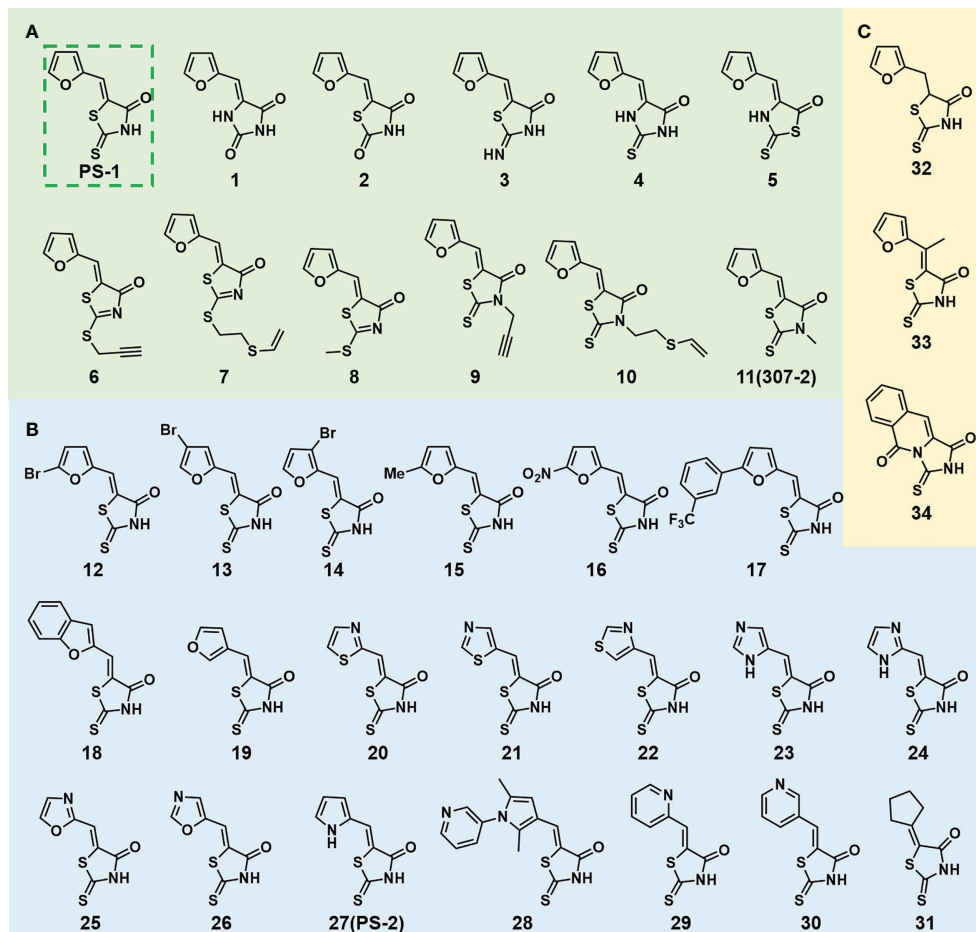


FIGURE 1

Synthesis of PS-1 analogs with altered functional groups. (A) PS-1 analogues with modifications on the rhodanine ring. (B) PS-1 analogs with modifications on the furan ring. (C) Other PS-1 analogs.

PM H^+ -ATPase following treatment with these analogs. The inhibitory effects of the PS-1 analogs on PM H^+ -ATPase activity in Arabidopsis plasma membrane vesicles were consistent with the inhibitory effects measured in the RS72 yeast system (Figure 2A, Supplementary Figure 1). The inhibitory effect of analog PS-2 was the strongest. Compared to the DMSO control, treatment with 5 μ M PS-2 inhibited approximately 85% of PM H^+ -ATPase activity, while the same concentration of PS-1 only inhibited ~44% of this activity (Figure 2A). To characterize the mode of H^+ -ATPase inhibition by PS-2, we measured enzyme kinetics in the presence of various concentrations of PS-2 (0.25, 0.5, 1 and 2.5 μ M), PS-1 (1, 2.5, 5 and 10 μ M) or 307-2 (10 μ M) with increasing concentrations of the substrate ATP (0.25–4 mM). Total PM H^+ -ATPase hydrolysis activity is shown in Figures 2B–D, and the initial plots indicated non-competitive inhibition, so the curves were fitted by appropriate nonlinear regression. Compared to control DMSO, K_m values for ATP remained relatively constant regardless of the addition of PS-2,

PS-1 or 307-2 (Supplementary Tables 1–3). On the other hand, V_{max} values decreased due to increasing concentration of PS-2, PS-1 or 307-2 (Supplementary Tables 1–3). These kinetic data suggest that PS-2 behaves as a noncompetitive inhibitor of ATP. We then determined the effect of PS-2 on the optimum pH for the hydrolytic activity of H^+ -ATPase. The results showed that the maximum activity of PM H^+ -ATPase was close to pH 6.5 in the presence or absence of PS-2 (Figure 2E).

Testing the ability of PS-1 analogs to inhibit PM H^+ -ATPase activity in yeast strain RS72 cells expressing Arabidopsis AHA2

To identify compounds that are stronger PM H^+ -ATPase inhibitors than PS-1, we screened the 34 PS-1 analogs by

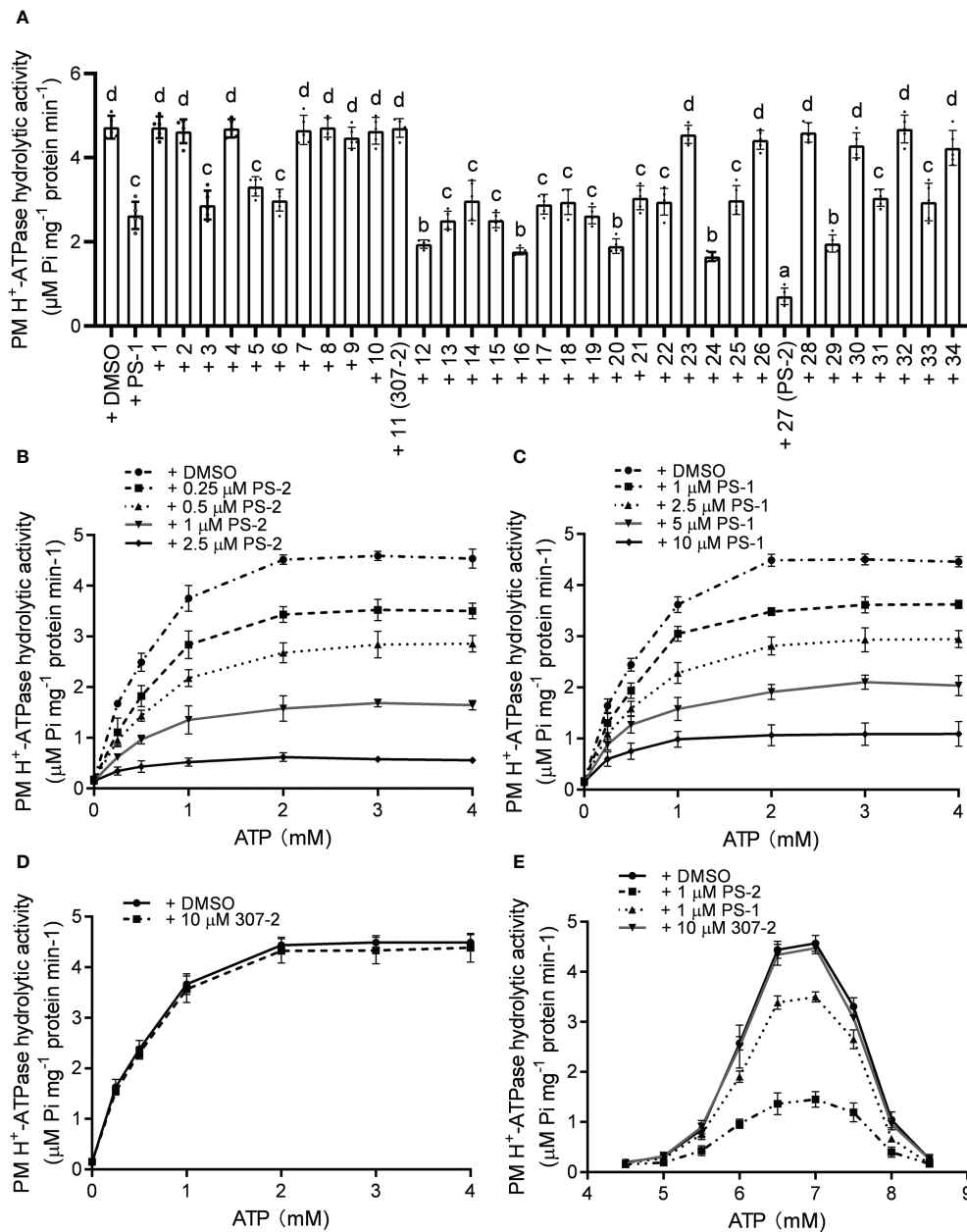


FIGURE 2

Effects of PS-2 on PM H⁺-ATPase hydrolytic activity. (A) Effects of PS-1 analogs on PM H⁺-ATPase hydrolytic activity. Plasma membrane vesicles were isolated from Arabidopsis Col-0 seedlings that were treated with 250 mM NaCl for 3 d before harvest. The inhibitory effects of 10 μM PS-1 analogs or 0.1% (v/v) DMSO on PM H⁺-ATPase hydrolytic activity were assessed. Data are means ± SD of five replicates. (B) Kinetic analysis of PM H⁺-ATPases inhibition by PS-2. (C) Kinetic analysis of PM H⁺-ATPases inhibition by PS-1. (D) Kinetic analysis of PM H⁺-ATPases inhibition by 307-2. (E) PM H⁺-ATPase activity assayed between pH 4.5 and pH 8.5 in the presence or absence of PS-2. Different lowercase letters indicate significant differences (P ≤ 0.05), as determined by one-way ANOVA.

observing their inhibitory effects on the growth of RS72 yeast cells expressing the Arabidopsis PM H⁺-ATPase AHA2. In RS72 yeast cells, the expression of *PMA1*, yeast's endogenous PM H⁺-ATPase gene, is controlled by the galactokinase 1 (*GAL1*) promoter. Although yeast contains two PM H⁺-ATPases, *PMA1* and *PMA2*, unlike *PMA1*, *PMA2* is expressed at low

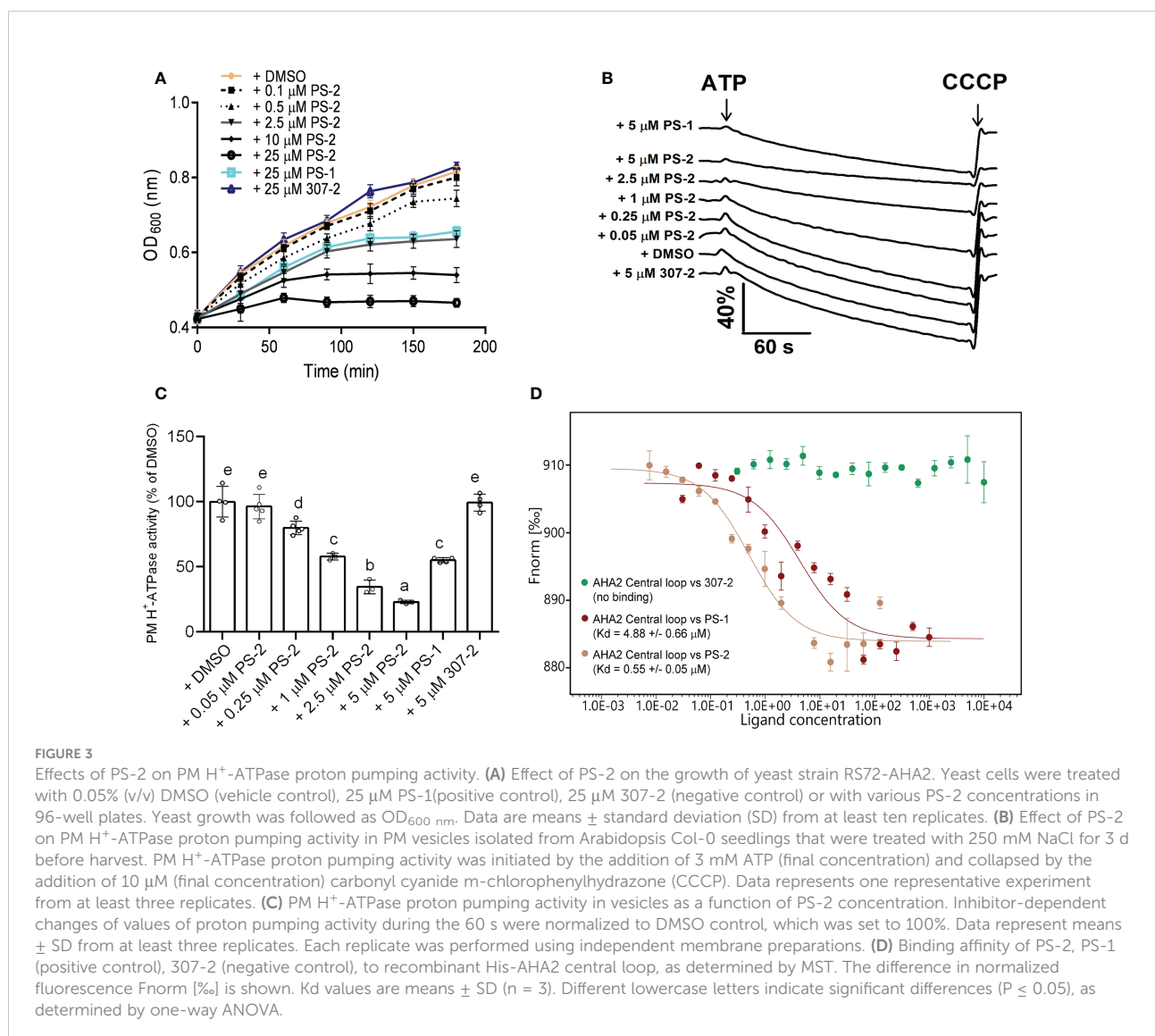
levels and is not required for yeast growth (Ghislain and Goffeau, 1991). RS72 yeast cannot survive on medium containing glucose as the sole carbon source, but heterologous expression of the Arabidopsis *AHA2* gene under the control of the yeast *PMA1* promoter (Villalba et al., 1992; Regenberget al., 1995) rescues this growth defect (Regenberget al., 1995; Kjellerup et al., 2017).

Inhibition of AHA2 activity in yeast strain RS72-AHA2 using PS-1 resulted in decreased yeast cell growth. Therefore, we performed a phenotypic screen of PS-1 analogs based on the growth of yeast RS72-AHA2 cells to identify PM H⁺-ATPase inhibitors that are more potent than PS-1. In an initial screen (Supplementary Figure 1), we identified several analogs that were more potent than PS-1 in inhibiting the growth of RS72 yeast, with PS-2 being the most potent. Furthermore, we measured a dose-dependent inhibition of yeast strain RS72-AHA2 by PS-2 (0.1–25 μ M) and proton pumping activity (0.05–5 μ M in isolated plasma membrane vesicles from Arabidopsis) (Figures 3A–C). The results of plasma membrane vesicles showed that PS-2 was about 5 times more effective than PS-1, and the inhibitory effect of 1 μ M PS-2 on PM H⁺-ATPase was comparable to that of 5 μ M PS-1 (Figure 3C). Besides, we also measured the binding constant between PS-2 and the AHA2

central loop using microscale thermophoresis (MST). A 10-fold boost in affinity between the AHA2 central loop and PS-2 interaction was observed ($K_d=0.55 \pm 0.05$) relative to the AHA2 central loop-PS-1 ($K_d=4.88 \pm 0.66$ μ M), while no measurable binding was detected between the 307-2 and AHA2 central loop (Figure 3D).

Effects of PS-1 analogs on Arabidopsis seedling growth

We previously demonstrated that PS-1 inhibits PM H⁺-ATPase activity and Arabidopsis seedling growth (Yang et al., 2022). In our screen of 34 PS-1 analogs, we identified several with stronger inhibitory effects than PS-1 on PM H⁺-ATPase activity (Supplementary Figure 1, Figure 2A). To further verify



the inhibitory effects of these analogs, we observed their effects (at 2.5 μM) on Arabidopsis seedling growth. As expected, the ability of the PS-1 analogs to inhibit PM H^+ -ATPase was consistent with their ability to inhibit Arabidopsis root growth: compounds that strongly inhibited PM H^+ -ATPase activity also strongly inhibited Arabidopsis root growth (Supplementary Figure 2), with analog PS-2 having the strongest inhibitory effect (Supplementary Figure 2, Figure 4A). In addition, we observed a dose-dependent inhibition of Arabidopsis seedling growth by PS-2 (0.5–4 μM). Specifically, PS-2 blocked primary root growth and fresh weight in a dose-dependent manner, and the inhibitory effect of 0.5 μM PS-2 was comparable to that of 4 μM PS-1 (Figures 4B–D).

The effect of PS-1 analog PS-2 on polar auxin transport

We previously demonstrated that PS-1 inhibits PM H^+ -ATPase activity and inhibits polar auxin transport in Arabidopsis roots (Yang et al., 2022). We observed that the PS-1 analog PS-2 had a significantly stronger inhibitory effect than PS-1 on PM H^+ -ATPase activity. To compare the effects of PS-2 and PS-1 on polar auxin transport, we examined ^3H -IAA transport and the expression of the auxin-responsive reporter gene *DR5-GFP* in Arabidopsis roots in the presence of these compounds. Compared to the DMSO control, the uptake of ^3H -IAA was significantly reduced in the presence of 5 μM PS-1 or PS-2 (Figure 5A). As expected, the inhibitory effect of PS-2 was significantly stronger than that of PS-1. The inhibitory effect of 1 μM PS-2 was similar to that of 5 μM PS-1, whereas 5 μM 307-2 (a PS-1 analog that did not significantly inhibit PM H^+ -ATPase activity) had no apparent effect on auxin uptake (Figure 5A). We also examined auxin transport in Arabidopsis roots treated with PS-2 or PS-1 by measuring their acropetal and basipetal polar transport of ^3H -IAA. Treatment with 5 μM PS-2 or PS-1 significantly reduced both acropetal and basipetal ^3H -IAA polar transport in roots, but the inhibitory effect of PS-2 was significantly stronger than that of PS-1 (Figures 5B, C). By contrast, 307-2 had no effect on polar ^3H -IAA transport (Figures 5B, C).

Finally, we measured the effects of PS-2 and PS-1 on the redistribution of auxin in response to gravity by examining the expression of the auxin reporter *DR5-GFP* in Arabidopsis roots. As expected, untreated roots expressed *DR5-GFP* asymmetrically under gravistimulation, with enhanced *DR5-GFP* expression in the outermost cell layer on the underside of the root tip (Figure 5D). In seedlings treated with PS-2 or PS-1, this localized enhancement of *DR5-GFP* expression was attenuated, and the inhibitory effect of PS-2 was significantly stronger than that of PS-1 (Figure 5D). By contrast, 307-2 had no effect on the asymmetric auxin accumulation in response to

gravity (Figure 4D). In roots exposed to 200 nM NAA (an auxin) for 4 hours, *DR5-GFP* was strongly expressed in the outer layer of both sides of the root tip. However, 1 μM PS-2 reduced the *DR5-GFP* signal induced by NAA treatment (Figure 5D). Taken together, these results indicate that PS-2 is a strong inhibitor of polar auxin transport.

Discussion

We synthesized 34 analogs of the PM H^+ -ATPase inhibitor PS-1 by systematically altering its functional groups and then screened these analogs for enhanced inhibitory activity. Structure-activity analysis showed that replacement of the rhodanine ring or modification of it compromised or totally abolished the inhibitory effects on both the yeast growth and the Arabidopsis seedling growth, suggesting the rhodanine is critical for the binding to PM H^+ -ATPase. Modification on the furan ring, however, is tolerable, and the introduction of an electron-withdrawing group (Bromo or nitro group) at the 5-position improved the inhibitory effect (compounds 12 and 16), while replacement of the furan ring with nitrogen-containing five-membered ring (compounds 20, 24, and 27), especially those with a hydrogen bond donor (24 and 27), markedly increased the potency. The analog 27, named PS-2, had the strongest inhibitory effects on PM H^+ -ATPase activity and polar auxin transport, and was clearly a stronger inhibitor than PS-1. Because it has a better inhibitory effect than PS-1, PS-2 should be a useful tool to study the biological functions of PM H^+ -ATPase.

We previously tested the effect of PM H^+ -ATPase activity on polar auxin transport by treating the roots of Arabidopsis seedlings with selective inhibitor PS-1 of PM H^+ -ATPase (Yang et al., 2022). The results supported the chemiosmotic model that PM H^+ -ATPase mediates polar auxin transport. In the current study, we identified PS-2, a PS-1 analog with a stronger inhibitory effect on PM H^+ -ATPase than PS-1. PS-2 inhibited the polar transport of auxin, further verifying the chemiosmotic model. PS-2 represents a potential tool to further explore the physiological roles of PM H^+ -ATPases.

Materials and methods

Plant materials

Arabidopsis thaliana Col-0 seeds were surface sterilized, germinated on Murashige and Skoog (MS) medium plus 0.6% (w/v) Phytigel (Sigma, lot # WXBC6825V) and 2.5% (w/v) sucrose, incubated in the dark at 4°C for 48 h, and vertically grown in a controlled growth chamber under a 16-h-light/8-h-dark cycle (22°C) for 5 d. The seedlings were transferred to

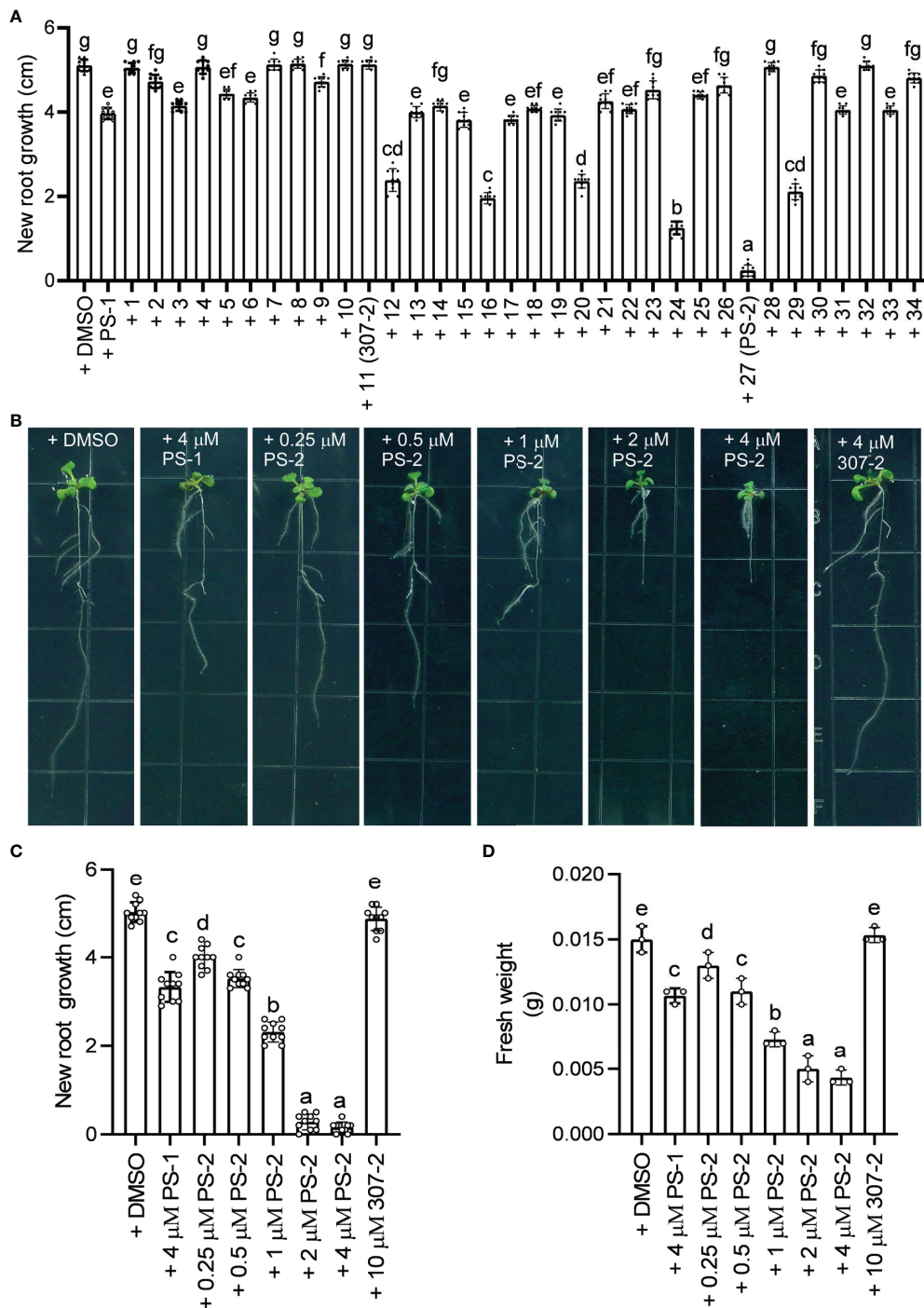


FIGURE 4
 Effects of PS-2 on Arabidopsis seedling growth. **(A)** New growth of primary roots shown in [Supplementary Figure 2](#) during the course of the experiment. Data are means \pm SD of 10 plants. Different lowercase letters indicate significant differences ($P \leq 0.05$), as determined by one-way ANOVA. **(B)** Representative photographs of PS-2-treated seedlings. Five-day-old seedlings grown on MS medium, pH 5.8, were transferred to plates containing indicated PS-2 or 0.05% (v/v) DMSO (vehicle control), 4 μ M PS-1 (positive control), 4 μ M 307-2 (negative control) and incubated for 7 d at 22°C for 7 d prior to photography. **(C)** Lengths of new growth primary roots in [Figure 3B](#) were measured 7 days after transfer. Data represent mean values \pm SD ($n = 10$ replicates). **(D)** Analysis of fresh weight for seedlings in [Figure 3B](#). Error bars represent SD ($n = 3$, 3 plates, 4 seedlings on each plate are weighed together) from the measurements using the same preparation.

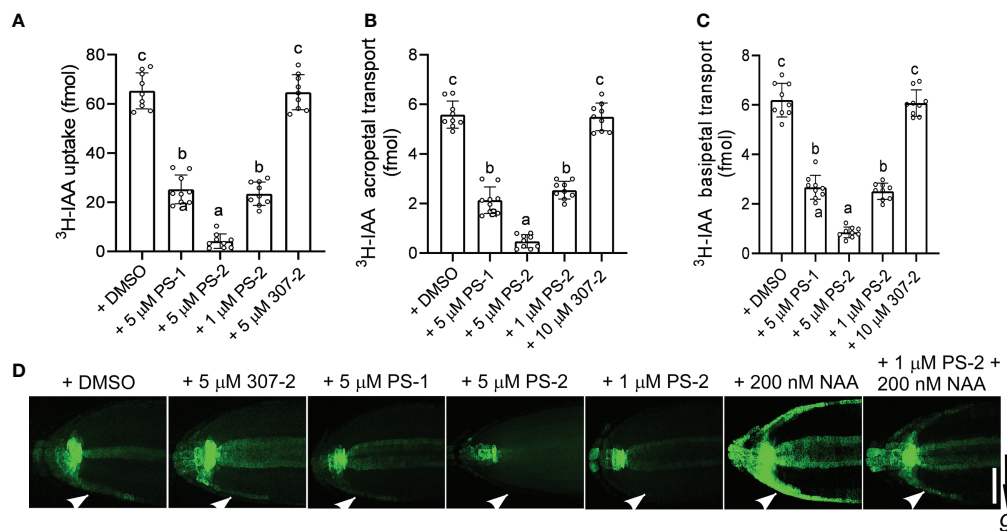


FIGURE 5

Effects of PS-1 analogs on polar auxin transport. **(A)** Uptake of ^3H -labeled IAA in root tips of Col-0 seedlings. Ten apical hypocotyl segments (each 5 mm long) were placed in 25 μL of buffer (5 nM ^3H -labeled IAA, 1 μM IAA, 1% [w/v] sucrose, and 5 mM sodium phosphate, pH 6.0) containing the indicated concentration of PS-1 analog (0.1% [v/v] DMSO as a control). After shaking for 2 h (100 rpm/min) at room temperature, the amount of ^3H -IAA in the segments was measured. Data are means \pm SD of 9 replicates. **(B, C)** Effects of PS-1 analogs on acropetal and basipetal transport of ^3H -labeled IAA in the roots of Arabidopsis Col-0 seedlings. Seven-day-old seedlings were placed on square agar plates containing the indicated concentration of PS-1 analog (0.1% [v/v] DMSO as a control). Agar pieces containing 100 nM ^3H -labeled IAA were placed below the shoot–root junction for 12 h (B, acropetal transport) or at the root tip for 6 h (C, basipetal transport). The amount of ^3H -labeled IAA in segments 5 mm from root tip (B) or from 10 to 15 mm (C) above the root apex was determined. Data are means \pm SD of 9 biological replicates. Different lowercase letters indicate significant differences ($P \leq 0.05$), as determined by one-way ANOVA. **(D)** Effects of PS-1 on asymmetric auxin accumulation in response to gravity. Seven-day-old *DR5:GFP* transgenic seedlings were placed on square agar plates containing the indicated concentration of PS-1 analog (or 0.1% [v/v] DMSO as a control) and rotated 90° for 4 h prior to imaging. One representative image is shown out of 10 seedlings imaged in the experiments. The arrow indicates the direction of gravity. Bar = 100 μm .

control plates (containing 0.1% [v/v] DMSO) or plates containing 2.5 μM PS-1 or PS-1 analogs (in 0.1% [v/v] DMSO) and incubated for 7 d under a 16-h-light/8-h-dark cycle (22°C).

Screening of PS-1 analogs and PS-2 dose-dependent inhibition assay

We screened PS-I analogs in yeast strain RS72 expressing Arabidopsis AHA2, which was constructed as previously reported (Regenberg et al., 1995). Yeast cells were pre-cultured in flasks to an OD_{600} of 0.5 and diluted at a ratio of 1:5 or 1:25 in fresh medium. A 4 μL aliquot of yeast cells was spotted onto solid medium containing DMSO as a control (0.1% [v/v]) or 10 μM PS-1 or PS-1 analog and photographed after 3 days of incubation at 28°C.

In the PS-2 dose-dependent inhibition assay against yeast strain RS72, yeast cells were pre-cultured in flasks until $\text{OD}_{600 \text{ nm}}$ reached approximately 0.4. Yeast cells were then aliquoted into 96-well plates, receiving 200 μL of culture per well in the presence of the DMSO control (0.1% [v/v]) or various compounds (0.1 to 25 μM of PS-2, 25 μM of PS-1 or 25 μM

of 307-2). Yeast growth ($\text{OD}_{600 \text{ nm}}$) was monitored using a microplate reader (Bio-Tek) after shaking at 28°C at 220 rpm/min for 3 h.

Assay of PM H^+ -ATPase hydrolytic activity and proton pumping activity

Plasma membrane-enriched vesicles were isolated from 3-week-old Arabidopsis seedlings using two-phase partitioning (Qiu et al., 2002; Yang et al., 2010). PM H^+ -ATPase hydrolytic activity was measured as described previously (Qiu et al., 2004) in the presence of the DMSO control (0.1% [v/v]) or 10 μM PS-1 or PS-1 analog. The proton pumping activity was measured in the presence of the DMSO control (0.1% [v/v]) or various compounds (0.05 to 5 μM of PS-2, 5 μM of PS-1 or 5 μM of 307-2) as described previously (Qiu et al., 2002).

Microscale thermophoresis assay

The interaction between the AHA2 central cyclic peptide and PS-2 was detected by MST analysis using the NanoTemper

Monolith NT.115 instrument as previously described (Wienken et al., 2010). Recombinant AHA2 central loop peptide was labeled with the Monolith NTTM Protein Labeling Kit RED (<http://www.nanotemper-technologies.com/>). The concentration of various compounds (PS-2, PS-1 or 307-2) ranged from 0.015 to 1000 μM . The labeled AHA2 central loop peptide was used in PBS buffer (10 nM in phosphate, pH 7.6) containing 0.05% (v/v) Tween 20 (PBST). The labeled peptide and compound mixture was incubated in PBST buffer for 5 min in the dark and then transferred to standard treated capillaries for measurement.

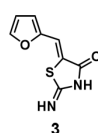
IAA transport assay

Auxin uptake in Arabidopsis roots was measured as previously described (Rahman et al., 2001). Assays for acropetal and basipetal transport of auxin in Arabidopsis roots were performed as described previously (Lewis and Muday, 2009).

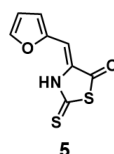
Synthetic schemes, methods, and characterizations

^1H NMR spectra were performed on a Varian or Bruker 400 MHz spectrometer at ambient temperature with CDCl_3 or DMSO-d_6 as the solvent unless otherwise addressed. ^{13}C NMR spectra were recorded on a Varian or Bruker 100 MHz spectrometer at ambient temperature (with complete proton decoupling). Chemical shifts are reported in parts per million relative to DMSO-d_6 (^1H , δ 2.50; ^{13}C , δ 39.50) or chloroform (^1H , δ 7.26; ^{13}C , δ 77.00). Data for ^1H NMR are reported as follows: chemical shift, multiplicity (s = singlet, d = doublet, m = multiplet), coupling constants and integration. High-resolution mass spectra were obtained at Peking University Mass Spectrometry Laboratory using Bruker APEX Flash chromatography. All chemical reagents were used as supplied by Alfa Aesar Chemicals, Sigma-Aldrich, J&K, and Acros. EtOH was distilled from calcium hydride; tetrahydrofuran (THF) was distilled from sodium/benzophenone prior to use. Compound 1-2, 4, 6, 8-9, 11, 15-18, 25, 28-31, 33-34 are the same as literature reported.

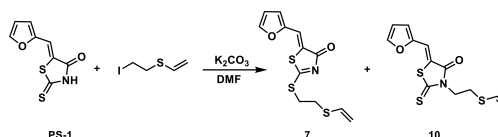
General procedure: To a solution of the aldehyde (1 equiv) and the heterocycle compound (1 equiv) in acetic acid was added ammonium acetate (2 equiv). The mixture was stirred at reflux under an argon atmosphere. After 4 h, the reaction mixture was cooled to room temperature and the precipitates were collected by filtration and washed with distilled water. The title compound was recrystallized in ethanol.



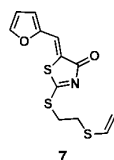
(Z)-5-(furan-2-ylmethylene)-2-iminothiazolidin-4-one(3): prepared according to general procedure with furfural and 2-iminothiazolidin-4-one to yield compound 3 (128.4 mg, 0.662 mmol, 77%). ^1H NMR (400 MHz DMSO-d_6): δ 6.69 (dd, $J = 3.2$ Hz, 1.6 Hz, 1H), 6.93 (d, $J = 3.6$ Hz, 1H), 7.39 (s, 1H), 7.95 (d, $J = 1.6$ Hz, 1H), 9.05 (br, 1H), 9.32 (br, 1H); ^{13}C NMR (100 MHz DMSO-d_6): δ 113.2, 115.8, 116.1, 126.9, 146.1, 149.7, 176.1, 180.1. HRMS (ESI): $[\text{M} + \text{H}]^+$ calculated for $\text{C}_8\text{H}_7\text{N}_2\text{O}_2\text{S}$: 195.0223, found: 195.0224.



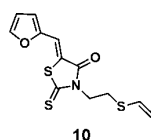
(Z)-4-(furan-2-ylmethylene)-2-thioxothiazolidin-5-one(5): prepared according to general procedure with furfural and 2-thioxothiazolidin-5-one to yield compound 5 (13.4 mg, 0.636 mmol, 63%). ^1H NMR (400 MHz DMSO-d_6): δ 6.65 (s, 1H), 6.75 (dd, $J = 3.6$ Hz, 2 Hz, 1H), 7.29 (d, $J = 3.6$ Hz, 1H), 8.01 (d, $J = 1.6$ Hz, 1H); ^{13}C NMR (100 MHz DMSO-d_6): δ 102.3, 113.8, 119.4, 131.0, 147.5, 148.4, 187.7, 188.2; HRMS (ESI): $[\text{M} + \text{H}]^+$ calculated for $\text{C}_8\text{H}_6\text{NO}_2\text{S}_2$: 211.9835, found: 211.9836.



To a solution of PS-1 (51 mg, 0.241 mmol) and (2-iodoethyl)vinylsulfane (77.4 mg, 0.362 mmol) in 2 mL of DMF was added K_2CO_3 (50 mg, 0.362 mmol). The mixture was stirred under the atmosphere of argon at room temperature overnight. The mixture was then concentrated in vacuo and the residue was purified by thin-layer chromatography to afford compounds 7 (53.9 mg, 0.181 mmol, 75.2%) and 10 (16.7 mg, 0.0562 mmol, 23.3%).



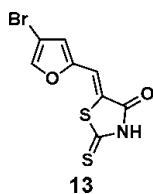
(Z)-5-(furan-2-ylmethylene)-2-((2-(vinylthio)ethyl)thio)thiazol-4(5H)-one (7): ^1H NMR (400 MHz CDCl_3): δ 3.12-3.17 (m, 2H), 3.58-3.63 (m, 2H), 5.29 (d, $J = 16.8$ Hz, 1H), 5.31 (d, $J = 10$ Hz, 1H), 6.35 (dd, $J = 16.8$ Hz, 10 Hz, 1H), 6.58 (dd, $J = 3.2$ Hz, 1.8 Hz, 1H), 6.82 (d, $J = 3.6$ Hz, 1H), 7.61 (s, 1H), 7.66 (m, 1H); HRMS (ESI): $[\text{M} + \text{H}]^+$ calculated for $\text{C}_{12}\text{H}_{12}\text{NO}_2\text{S}_3$: 298.0025, found: 298.0029.



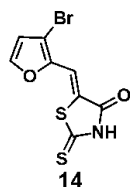
(Z)-5-(furan-2-ylmethylene)-2-thioxo-3-(2-(vinylthio)ethyl)thiazolidin-4-one (10): ^1H NMR (400 MHz CDCl_3): δ 3.01 (t, $J = 7.4$ Hz, 2H), 4.34 (t, $J = 7.4$ Hz, 2H), 5.29 (d, $J = 10$ Hz, 1H), 5.35 (d, $J = 16.8$ Hz, 1H), 6.36 (dd, $J = 16.8$ Hz, 10 Hz, 1H), 6.60 (m, 1H), 6.85 (d, $J = 3.6$ Hz, 1H), 7.48 (s, 1H), 7.71 (s, 1H); ^{13}C NMR (100 MHz CDCl_3): δ 27.6, 43.2, 112.5, 113.6, 118.6, 118.9, 120.5, 130.6, 147.2, 150.0, 167.3, 194.3; HRMS (ESI): $[\text{M} + \text{H}]^+$ calculated for $\text{C}_{12}\text{H}_{12}\text{NO}_2\text{S}_3$: 298.0025, found: 298.0027.



(Z)-5-((5-bromofuran-2-yl)methylene)-2-thioxothiazolidin-4-one (12): prepared according to general procedure with 5-bromofuran-2-carbaldehyde and rhodanine to yield compound 12 (53 mg, 0.262 mmol, 64%). ^1H NMR (400 MHz DMSO-d_6): δ 6.91 (d, $J = 4$ Hz, 1H), 7.20 (d, $J = 3.6$ Hz, 1H), 7.42 (s, 1H), 13.75 (br, 1H); ^{13}C NMR (100 MHz DMSO-d_6): δ 116.0, 116.3, 121.7, 123.2, 128.0, 151.5, 168.9, 196.1; HRMS (ESI): $[\text{M} + \text{H}]^+$ calculated for $\text{C}_8\text{H}_5\text{BrNO}_2\text{S}_2$: 289.8940, found: 289.8942.

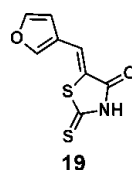


(Z)-5-((4-bromofuran-2-yl)methylene)-2-thioxothiazolidin-4-one (13): prepared according to general procedure with 4-bromofuran-2-carbaldehyde and rhodanine to yield compound 13 (133 mg, 0.332 mmol, 81%). ^1H NMR (400 MHz DMSO-d_6): δ 7.31 (d, $J = 2$ Hz, 1H), 7.42 (s, 1H), 8.34 (s, 1H), 13.78 (br, 1H); ^{13}C NMR (100 MHz DMSO-d_6): δ 102.5, 116.3, 120.8, 124.5, 146.0, 150.3, 168.9, 196.2, HRMS (ESI): $[\text{M} + \text{H}]^+$ calculated for $\text{C}_8\text{H}_5\text{BrNO}_2\text{S}_2$: 289.8940, found: 289.8942.

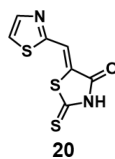


(Z)-5-((3-bromofuran-2-yl)methylene)-2-thioxothiazolidin-4-one (14): prepared according to general procedure with 3-bromofuran-2-carbaldehyde and rhodanine to yield compound 14 (53.9 mg, 0.188 mmol, 59%). ^1H NMR (400 MHz DMSO-d_6): δ 7.06 (d, $J = 2$ Hz, 1H), 7.17 (s, 1H), 8.20 (d, $J = 2$ Hz, 1H), 12.92 (br, 1H); ^{13}C NMR (100 MHz DMSO-d_6): δ 108.9, 112.9, 116.8, 124.9, 146.6, 148.9, 169.0,

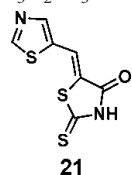
196.1; HRMS (ESI): $[\text{M} + \text{H}]^+$ calculated for $\text{C}_8\text{H}_4\text{BrNO}_2\text{S}_2$: 289.8940, found: 289.8943.



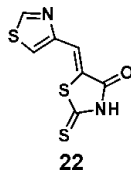
(Z)-5-(furan-3-ylmethylene)-2-thioxothiazolidin-4-one (19): prepared according to general procedure with furan-3-carbaldehyde and rhodanine to yield compound 19 (58.4 mg, 0.277 mmol, 74%). ^1H NMR (400 MHz DMSO-d_6): δ 6.78 (d, $J = 2$ Hz, 1H), 7.58 (s, 1H), 7.91 (m, 1H), 8.32 (s, 1H), 13.75 (bs, 1H); ^{13}C NMR (100 MHz DMSO-d_6): δ 109.4, 121.4, 123.4, 124.9, 146.5, 148.6, 169.5, 195.6; HRMS (ESI): $[\text{M} + \text{H}]^+$ calculated for $\text{C}_8\text{H}_6\text{NO}_2\text{S}_2$: 211.9835, found: 211.9835.



(Z)-5-(thiazol-2-ylmethylene)-2-thioxothiazolidin-4-one (20): prepared according to general procedure with thiazole-2-carbaldehyde and rhodanine to yield compound 20 (98 mg, 0.429 mmol, 97%). ^1H NMR (400 MHz DMSO-d_6): δ 7.91 (s, 1H), 8.09 (d, $J = 3.2$ Hz, 1H), 8.21 (d, $J = 3.2$ Hz, 1H), 13.79 (br, 1H); ^{13}C NMR (100 MHz DMSO-d_6): δ 119.9, 125.4, 129.3, 145.4, 160.7, 168.9, 199.7; HRMS (ESI): $[\text{M} + \text{H}]^+$ calculated for $\text{C}_7\text{H}_5\text{N}_2\text{OS}_3$: 228.9559, found: 228.9561.

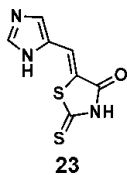


(Z)-5-(thiazol-5-ylmethylene)-2-thioxothiazolidin-4-one (21): prepared according to general procedure with thiazole-5-carbaldehyde and rhodanine to yield compound 21 (83.8 mg, 0.367 mmol, 83%). ^1H NMR (400 MHz DMSO-d_6): δ 8.03 (m, 1H), 8.05 (m, 1H), 9.46 (s, 1H), 13.95 (br, 1H); ^{13}C NMR (100 MHz DMSO-d_6): δ 121.6, 126.9, 123.1, 149.4, 159.7, 168.6, 194.2; HRMS (ESI): $[\text{M} + \text{H}]^+$ calculated for $\text{C}_7\text{H}_5\text{N}_2\text{OS}_3$: 228.9559, found: 228.9561.

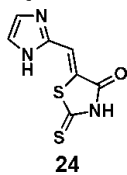


(Z)-5-(thiazol-4-ylmethylene)-2-thioxothiazolidin-4-one (22): prepared according to general procedure with thiazole-4-carbaldehyde and rhodanine to yield compound 22 (84.8 mg, 0.371 mmol, 84%). ^1H NMR (400 MHz DMSO-d_6): δ 7.70 (s, 1H), 8.40 (m, 1H), 9.34 (d, $J = 1.2$ Hz, 1H), 13.63 (bs, 1H); ^{13}C NMR (100 MHz DMSO-d_6): δ 122.7, 127.0, 127.4, 150.1, 156.3,

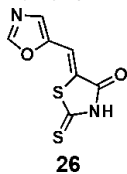
169.4, 199.4; HRMS (ESI): $[M + H]^+$ calculated for $C_7H_5N_2OS_3$: 228.9559, found: 228.9561.



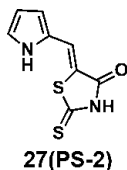
(Z)-5-((1*H*-imidazol-5-yl)methylene)-2-thioxothiazolidin-4-one(23): prepared according to general procedure with 1*H*-imidazole-5-carbaldehyde and rhodanine to yield compound 23 (251.4 mg, 0.2444 mmol, 47%). 1H NMR (400 MHz DMSO- d_6): δ 7.53 (s, 1H), 7.84 (d, 1H), 7.96 (s, 1H), 12.75 (br, 1H), 13.40 (br, 1H); ^{13}C NMR (100 MHz DMSO- d_6): δ 121.3, 124.1, 124.5, 135.7, 138.5, 169.4, 199.7. HRMS (ESI): $[M + H]^+$ calculated for $C_7H_6N_3OS_2$: 211.9947, found: 211.9948.



(Z)-5-((1*H*-imidazol-2-yl)methylene)-2-thioxothiazolidin-4-one(24): prepared according to general procedure with 1*H*-imidazole-2-carbaldehyde and rhodanine to yield compound 24 (5.9 mg, 0.123 mmol, 23.7%). 1H NMR (400 MHz DMSO- d_6): δ 7.32 (s, 1H), 7.35 (s, 1H), 7.50 (s, 1H), 12.93 (bs, 1H), 13.50 (bs, 1H); ^{13}C NMR (100 MHz DMSO- d_6): δ 116.7, 121.0, 125.6, 132.5, 142.0, 169.1, 199.7; HRMS (ESI): $[M + H]^+$ calculated for $C_7H_6N_3OS_2$: 211.9947, found: 211.9948.

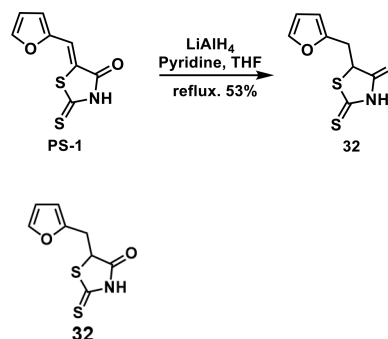


(Z)-5-(oxazol-5-ylmethylene)-2-thioxothiazolidin-4-one (26): prepared according to general procedure with oxazole-5-carbaldehyde and rhodanine to yield compound 26 (69.8 mg, 0.33 mmol, 64%). 1H NMR (400 MHz DMSO- d_6): δ 7.59 (s, 1H), 7.79 (s, 1H), 8.74 (s, 1H), 13.80 (br, 1H); ^{13}C NMR (100 MHz DMSO- d_6): δ 114.6, 126.0, 133.2, 146.8, 155.0, 168.8, 196.0; HRMS: $[M + H]^+$ calculated for $C_7H_5N_2O_2S_2$: 212.9787, found: 212.9789.



(Z)-5-((1*H*-pyrrol-2-yl)methylene)-2-thioxothiazolidin-4-one (27): prepared according to general procedure with 1*H*-pyrrole-

2-carbaldehyde and rhodanine to yield compound 27 (53 mg, 0.262 mmol, 64%). 1H NMR (400 MHz DMSO- d_6): δ 6.37 (m, 1H), 6.50 (m, 1H), 7.30 (m, 1H), 11.77 (br, 1H), 13.50 (br, 1H); ^{13}C NMR (100 MHz DMSO- d_6): δ 112.7, 115.0, 116.9, 121.9, 125.8, 127.2, 169.2, 194.8; HRMS: $[M + H]^+$ calculated for $C_8H_7N_2OS_2$: 210.9994, found: 210.9997.



5-(furan-2-ylmethyl)-2-thioxothiazolidin-4-one(32): To a solution of PS-1 (50 mg, 0.24 mmol) in THF/pyridine(1:1, 1 mL) was added 260 μ L of $LiAlH_4$ solution in THF(2 M). The mixture was stirred at reflux under the atmosphere of argon overnight. Then, the mixture was quenched by slowly adding 2M HCl solution. The mixture was extracted by ethyl acetate for 3 times. The combined organic layer was washed with brine, dried over *anhyd.* Na_2SO_4 and concentrated *in vacuo*. The residue was purified by column chromatography to give 32 as a brown solid (26.8 mg, 0.126 mmol, 53%). 1H NMR (400 MHz $CDCl_3$): δ 3.28 (dd, $J = 15.6$ Hz, 9.6 Hz, 1H), 3.55 (dd, $J = 15.6$ Hz, 4 Hz, 1H), 4.66(dd, $J = 9.6$ Hz, 4 Hz, 1H), 6.18 (d, $J = 3.6$ Hz, 1H), 6.32 (dd, $J = 3.2$ Hz, 1.6 Hz, 1H), 7.36 (d, $J = 2$ Hz 1H), 9.39 (br, 1H); ^{13}C NMR (100 MHz $CDCl_3$): δ 31.0, 53.7, 108.2, 110.6, 142.6, 149.4, 176.1, 200.0; HRMS: $[M + H]^+$ calculated for $C_8H_8NO_2S_2$: 213.9991, found: 213.9993.

Data availability statement

The original contributions presented in the study are included in the article/[Supplementary Material](#). Further inquiries can be directed to the corresponding authors.

Author contributions

YY, LiX, WX, LW, ML, LX, FH, SS, and LeX designed the research. YY, LiX, WX, LW, ML, LX, FH, and SS conducted the research. YY, LiX, and LeX analyzed the data. YY, LiX, and LeX wrote and edited the manuscript

Funding

This work was supported by the National Natural Science Foundation of China (31872659, 32070301), the National Genetically Modified Organisms Breeding Major Projects (2016ZX08009002) and Exploration project of Center for Practical Courses in the Life Sciences of China Agricultural University (20210102, 20210103).

Conflict of interest

The authors declare that the research was conducted in the absence of any commercial or financial relationships that could be construed as a potential conflict of interest.

References

- Anfang, M., and Shani, E. (2021). Transport mechanisms of plant hormones. *Curr. Opin. Plant Biol.* 63, 102055. doi: 10.1016/j.pbi.2021.102055
- Baxter, I., Tchieu, J., Sussman, M. R., Boutry, M., Palmgren, M. G., Gribskov, M., et al. (2003). Genomic comparison of p-type ATPase ion pumps in arabidopsis and rice. *Plant Physiol.* 132, 618–628. doi: 10.1104/pp.103.021923
- Casanova-Sáez, R., Mateo-Bonmatí, E., and Ljung, K. (2021). Auxin metabolism in plants. *Cold Spring Harb. Perspect. Biol.* 13, a039867. doi: 10.1101/cshperspect.a039867
- Chen, X., Ding, Y., Yang, Y., Song, C., Wang, B., Yang, S., et al. (2021). Protein kinases in plant responses to drought, salt, and cold stress. *J. Integr. Plant Biol.* 63 (1), 53–78. doi: 10.1111/jipb.13061
- Falhof, J., Pedersen, J. T., Fuglsang, A. T., and Palmgren, M. (2016). Plasma membrane h^+ -ATPase regulation in the center of plant physiology. *Mol. Plant* 9 (3), 323–337. doi: 10.1016/j.molp.2015.11.002
- Gaxiola, R. A., Palmgren, M. G., and Schumacher, K. (2007). Plant proton pumps. *FEBS Lett.* 581, 2204–2214. doi: 10.1016/j.febslet.2007.03.050
- Ghislain, M., and Goffeau, A. (1991). The *pma1* and *pma2* h^+ -ATPases from *Schizosaccharomyces pombe* are functionally interchangeable. *J. Biol. Chem.* 266, 18276–18279. doi: 10.1016/S0021-9258(18)55265-0
- Han, X., Yang, Y., Wu, Y., Liu, X., Lei, X., and Guo, Y. (2017). A bioassay-guided fractionation system to identify endogenous small molecules that activate plasma membrane h^+ -ATPase activity in arabidopsis. *J. Exp. Bot.* 68, 2951–2962. doi: 10.1093/jxb/erx156
- Havshoi, N. W., and Fuglsang, A. T. (2022). A critical review on natural compounds interacting with the plant plasma membrane h^+ -ATPase and their potential as biologicals in agriculture. *J. Integr. Plant Biol.* 64 (2), 268–286. doi: 10.1111/jipb.13221
- Houlné, G., and Boutry, M. (1994). Identification of an *Arabidopsis thaliana* gene encoding a plasma membrane h^+ -ATPase whose expression is restricted to anther tissue. *Plant J.* 5, 311–317. doi: 10.1111/j.1365-313X.1994.00311.x
- Kerr, I. D., and Bennett, M. J. (2007). New insight into the biochemical mechanisms regulating auxin transport in plants. *Biochem. J.* 401, 613–622. doi: 10.1042/BJ20061411
- Kjellerup, L., Gordon, S., Cohrt, K. O., Brown, W. D., Fuglsang, A. T., and Winther, A. L. (2017). Identification of antifungal h^+ -ATPase inhibitors with effect on plasma membrane potential. *Antimicrob. Agents Chemother.* 61, e00032-17. doi: 10.1128/AAC.00032-17
- Kramer, E. M., and Bennett, M. J. (2006). Auxin transport: A field in flux. *Trends Plant Sci.* 11, 382–386. doi: 10.1016/j.tplants.2006.06.002
- Lewis, D. R., and Muday, G. K. (2009). Measurement of auxin transport in arabidopsis thaliana. *Nat. Protoc.* 4, 437–451. doi: 10.1038/nprot.2009.1
- Lin, W., Zhou, X., Tang, W., Takahashi, K., Pan, X., Dai, J., et al. (2021). TMK-based cell-surface auxin signalling activates cell-wall acidification. *Nature* 599, 278–282. doi: 10.1038/s41586-021-03976-4
- Li, L., Verstraeten, I., Roosjen, M., Takahashi, K., Rodriguez, L., Merrin, J., et al. (2021). Cell surface and intracellular auxin signalling for h^+ fluxes in root growth. *Nature* 599, 273–277. doi: 10.1038/s41586-021-04037-6
- Mito, N., Wimmers, L. E., and Bennett, A. B. (1996). Sugar regulates mRNA abundance of h^+ -ATPase gene family members in tomato. *Plant Physiol.* 112, 1229–1236. doi: 10.1104/pp.112.3.1229
- Muday, G. K., and DeLong, A. (2001). Polar auxin transport: controlling where and how much. *Trends Plant Sci.* 6, 535–542. doi: 10.1016/S1360-1385(01)02101-X
- Oufattole, M., Arango, M., and Boutry, M. (2000). Identification and expression of three new nicotiana plumbaginifolia genes which encode isoforms of a plasma membrane h^+ -ATPase, and one of which is induced by mechanical stress. *Planta* 210, 715–722. doi: 10.1007/s004250050672
- Palmgren, M. G. (2001). Plant plasma membrane h^+ -ATPases: powerhouses for nutrient uptake. *Annu. Rev. Plant Phys.* 52, 817–845. doi: 10.1146/annurev.arplant.52.1.817
- Parry, G., Delbarre, A., Marchant, A., Swarup, R., Napier, R., Perrot-Rechenmann, C., et al. (2001). Novel auxin transport inhibitors phenocopy the auxin influx carrier mutation aux1. *Plant J.* 25 (4), 399–406. doi: 10.1046/j.1365-313x.2001.00970.x
- Perrot-Rechenmann, C., and Bennett, M. J. (2001). Novel auxin transport inhibitors phenocopy the auxin influx carrier mutation aux1. *Plant J.* 25, 399–406. doi: 10.1046/j.1365-313x.2001.00970.x
- Qiu, Q. S., Guo, Y., Dietrich, M. A., Schumaker, K. S., and Zhu, J. K. (2002). Regulation of SOS-1, a plasma membrane Na^+/H^+ exchanger in *Arabidopsis thaliana*, by SOS2 and SOS3. *Proc. Natl. Acad. Sci. U.S.A.* 99, 8436–8441. doi: 10.1073/pnas.122224699
- Qiu, Q., Guo, Y., Quintero, F., Pardo, J., Schumaker, K., and Zhu, J. K. (2004). Regulation of vacuolar Na^+/H^+ exchange in arabidopsis thaliana by the SOS pathway. *J. Biol. Chem.* 279, 207–125. doi: 10.1074/jbc.M307982200
- Rahman, A., Ahamed, A., Amakawa, T., Goto, N., and Tsurumi, S. (2001). Chromosaponin I specifically interacts with AUX1 protein in regulating the gravitropic response of arabidopsis roots. *Plant Physiol.* 125, 990–1000. doi: 10.1104/pp.125.2.990
- Raven, J. A. (1975). Transport of indoleacetic acid in plant cells in relation to pH and electrical potential gradients, and its significance for polar IAA transport. *New Phytol.* 74, 163–172. doi: 10.1111/j.1469-8137.1975.tb02602.x
- Regenberg, B., Villalba, J. M., Lanfermeijer, F. C., and Palmgren, M. G. (1995). C-terminal deletion analysis of plant plasma membrane h^+ -ATPase: yeast as a model system for solute transport across the plant plasma membrane. *Plant Cell* 7, 1655–1666. doi: 10.1105/tpc.7.10.1655
- Rubery, P. H., and Sheldrake, A. R. (1974). Carrier-mediated auxin transport. *Planta* 118 (2), 101–121. doi: 10.1007/BF00388387
- Sperandio, M. V., Santos, L. A., Bucher, C. A., Fernandes, M. S., and de Souza, S. R. (2011). Isoforms of plasma membrane h^+ -ATPase in rice root and shoot are

Publisher's note

All claims expressed in this article are solely those of the authors and do not necessarily represent those of their affiliated organizations, or those of the publisher, the editors and the reviewers. Any product that may be evaluated in this article, or claim that may be made by its manufacturer, is not guaranteed or endorsed by the publisher.

Supplementary material

The Supplementary Material for this article can be found online at: <https://www.frontiersin.org/articles/10.3389/fpls.2022.973471/full#supplementary-material>

- differentially induced by starvation and resupply of NO_3^- or NH_4^+ . *Plant Sci.* 180, 251–258. doi: 10.1016/j.plantsci.2010.08.018
- Villalba, J. M., Palmgren, M. G., Berberian, G. E., Ferguson, C., and Serrano, R. (1992). Functional expression of plant plasma membrane h^+ -ATPase in yeast endoplasmic reticulum. *J. Biol. Chem.* 267, 12341–12349. doi: 10.1016/S0021-9258(19)49845-1
- Went, F. W. (1974). Reflections and speculations. *Annu. Rev. Plant Physiol.* 25, 1–26.
- Wienken, C. J., Baaske, P., Rothbauer, U., Braun, D., and Duhr, S. (2010). Protein binding assays in biological liquids using microscale thermophoresis. *Nat. Commun.* 1, 100. doi: 10.1038/ncomms1093
- Xi, D., Chen, X., Wang, Y., Zhong, R., He, J., Shen, J., et al. (2019). Arabidopsis ANAC092 regulates auxin-mediated root development by binding to the ARF8 and PIN4 promoters. *J. Integr. Plant Biol.* 61, 1015–1031. doi: 10.1111/jipb.12735
- Yang, Y., and Guo, Y. (2018a). Elucidating the molecular mechanisms mediating plant salt-stress responses. *New Phytol.* 217, 523–539. doi: 10.1111/nph.14920
- Yang, Y., and Guo, Y. (2018b). Unraveling salt stress signaling in plants. *J. Integr. Plant Biol.* 60, 796–804. doi: 10.1111/jipb.12689
- Yang, Y., Hammes, U. Z., Taylor, C. G., Schachtman, D. P., and Nielsen, E. (2006). High-affinity auxin transport by the AUX1 influx carrier protein. *Curr. Biol.* 16, 1123–1127. doi: 10.1016/j.cub.2006.04.029
- Yang, Y., Han, X., Ma, L., Wu, Y., Liu, X., Fu, H., et al. (2021). Dynamic changes of phosphatidylinositol and phosphatidylinositol 4-phosphate levels modulate h^+ -ATPase and Na^+/H^+ antiporter activities to maintain ion homeostasis in arabidopsis under salt stress. *Mol. Plant* 14, 2000–2014. doi: 10.1016/j.molp.2021.07.020
- Yang, Y., Liu, X., Guo, W., Liu, W., Shao, W., Zhao, J., et al. (2022). Testing the polar auxin transport model with a selective plasma membrane h^+ -ATPase inhibitor. *J. Integr. Plant Biol.* 64 (6), 1229–1245. doi: 10.1111/jipb.13256
- Yang, Y., Qin, Y., Xie, C., Zhao, F., Zhao, J., Liu, D., et al. (2010). The arabidopsis chaperone J3 regulates the plasma membrane h^+ -ATPase through interaction with the PKS5 kinase. *Plant Cell* 22, 1313–1332. doi: 10.1105/tpc.109.069609
- Yang, Z., Wang, C., Xue, Y., Liu, X., Chen, S., Song, C., et al. (2019a). Calcium-activated 14-3-3 proteins as a molecular switch in salt stress tolerance. *Nat. Commun.* 10, 1199. doi: 10.1038/s41467-019-09181-2
- Yang, Y., Wu, Y., Ma, L., Yang, Z., Dong, Q., Li, Q., et al. (2019b). The Ca^{2+} sensor ScaBP3/CBL7 modulates plasma membrane h^+ -ATPase activity and promotes alkali tolerance in arabidopsis. *Plant Cell* 31, 1367–1384. doi: 10.1105/tpc.18.00568
- Yu, Z., Zhang, F., Friml, J., and Ding, Z. (2022). Auxin signaling: research advances over the past 30 years. *J. Integr. Plant Biol.* 64, 371–392. doi: 10.1111/jipb.13225
- Zařimalová, E., Murphy, A. S., Yang, H., Hoyerová, K., and Hošek, P. (2010). Auxin transporters—why so many? cold spring harb perspect. *Biol* 2, a001552. doi: 10.1101/cshperspect.a001552